

PACS numbers: 61.72. – y, 75.50.Tt

**STRUCTURAL FEATURES OF NANOCRYSTALLINE MAGNETITE
OBTAINED BY DIFFERENT SYNTHESIS ACCORDING TO THE X-RAY
DIFFRACTION AND ELECTRON MICROSCOPY DATA**

S.N. Danilchenko¹, ***V.N. Kuznetsov***¹, ***A.S. Stanislavov***¹, ***O.V. Kalinkevich***¹,
A.N. Kalinkevich¹, ***M.G. Demidenko***², ***K.V. Tischenko***², ***L.F. Sukhodub***¹

¹ Institute of Applied Physics, National Academy of Sciences of Ukraine,
58, Petropavlovskaya Str., 40030 Sumy, Ukraine
E-mail: danil@ipflab.sumy.ua

² Sumy State University,
2, Rimsky-Korsakov Str., 40007 Sumy, Ukraine

Structural features of nanosized magnetite Fe₃O₄ synthesized in the presence of polymeric matrices (polysaccharide chitosan, etc.) were studied using transmission electron microscopy (TEM) and X-ray diffraction (XRD) analysis. The data obtained strongly suggest the influence of the polysaccharide matrix on the magnetite nanoparticles growth inhibition and size stabilization. The controlled size decrease of Fe₃O₄ nanoparticles is accompanied by the increase in the crystal lattice imperfection and the decrease in the unit cell size. The utility of TEM and XRD complementary use for the determination of nanosized magnetite particles structure and substructure parameters is shown in the present paper.

Keywords: MAGNETIC NANOPARTICLES, BIOPOLYMER MATRIX, CHITOSAN, XRD, TEM, PARTICLES SIZE.

(Received 29 June 2011, in final form 31 October 2011, online 05 November 2011)

1. INTRODUCTION

At present, materials based on nanosized Fe₃O₄ magnetite particles find wide application in the modern medicine [1-4] and technics [4-6]. When developing methods of production of such materials, control of the nanoparticle size is the key question, since all fields of application of nanomaterials on the basis of Fe₃O₄ are based on the strong dependences of the service properties on the sizes and degree of monodispersity of particles. A great attention is paid to both technological methods which allow to avoid agglomeration (coalescence) of magnetite nanoparticles and tool techniques of the determination of their dimensions and size distribution.

The known methods of magnetite nanoparticle stabilization are, for example, the following: formation of oriented layers of polarized organic molecules on the particle surface [3-4], use of the chelate effect of biomolecules [7-8], or synthesis in biopolymer matrix [9]. Many works have been published which describe the application of polysaccharides, in particular, chitosan, as an effective stabilizing agents for magnetite nanoparticles [7-8, 10-13]. Chitosan and its derivatives are widely used in the production of different biomedical materials due to the remarkable biological and chemical properties [14-16]. Presence of reactive groups (radicals) OH⁻ and NH₂⁻ allows to suggest the possibility of operation of the magnetite nanoparticle growth inhibition (stabilization) mechanisms in the presence of chitosan micromolecules.

Direct measurements using transmission electron microscopy (TEM) [17-18] and indirect ones, i.e. determination of the effective crystallite sizes by the analysis of the line broadening of X-ray diffraction [19-21], are the most widespread among the methods for estimating nanoparticle size. In the first case, both measurement errors and high probability of the subjective choice of insufficiently representative array of nanoparticles are the source of errors. In the case of the analysis of diffraction profile we determine some effective crystallite size averaged over the radiation area or the so-called coherent-scattering regions. Moreover, the majority of researchers ignore the fact that lattice microdeformations contribute to the broadening of diffraction lines together with high dispersity of crystallites. Taking into account the volume-surface ratio, which is very small for nanoparticles, and complex conditions of synthesis with the participation of surface-active agents, one can expect significant levels of microdeformations and structural distortions in nanocrystalline magnetites. It is known that the decrease in the nanoparticle size lower than some threshold value can provoke undesirable size effects which distort structural characteristics and increase concentration of linear and point defect that, in turn, influences the magnetic properties [8, 9, 11].

At present, a number of works which simultaneously use TEM and XRD for the size determination of magnetite nanocrystallites synthesized in biopolymer matrix is very small; and investigations taking into account multifactority of the physical broadening of diffraction lines are almost absent.

The aim of the present work consisted in combined and complementary use of the XRD and TEM methods for the size determination of magnetite nanocrystallites (L) considering the contribution of the average relative lattice microdeformation (ε) to the broadening of diffraction lines. Investigations were performed on a set of samples of magnetite and composite materials based on chitosan and magnetite obtained during the development and optimization of the methods of Fe_3O_4 chemical synthesis with controlled sizes and nanoparticle shape. In whole, the work is focused on the development of the magnetite-based nanocomposite materials technologies and tool methods of their approval.

2. MATERIALS AND METHODS

Synthetic magnetite (Fe_3O_4) was obtained by the deposition in alkaline medium (5% NaOH) from saline solutions of ferric and ferrous iron $\text{FeCl}_3 \cdot 6\text{H}_2\text{O}$ and $(\text{NH}_4)_2\text{SO}_4 \cdot \text{FeSO}_4 \cdot 6\text{H}_2\text{O}$, mole ratio of the salts is 1:2,41, time of synthesis is 2 min. Temperature of synthesis was 100°C for the sample "Magnetite 1" and 80°C – for the sample "Magnetite 2". Obtained powder was properly washed by decantation and dried. During decantation sample "Magnetite 2" was under the action of constant magnetic field. Sample "Magnetite 0" was obtained by classical thermochemical method [22] and used in the sequel for the comparison as a sample with relatively large sizes of crystalline particles.

Magnetite samples in biopolymer matrix were obtained by the addition of saline solutions of ferrous and ferric iron to 0,5% solution of low-molecular chitosan in 1% acetic acid (mole ratio of the salts is 2,41:1, chitosan-to-magnetite ratio is 50:50). Codeposition was performed by the addition of (1) mother solution to boiling NaOH (sample "Chit Fe_3O_4 "), (2) 5% NaOH at the temperature 80°C (sample "Chit $\text{Fe}_3\text{O}_4\text{NaOH}$ ") or (3) 10% NH_3 at room temperature (sample "Chit $\text{Fe}_3\text{O}_4\text{NH}_3$ ") to mother solution. Samples were washed by decantation and then dried.

X-ray diffraction investigation of synthesized materials were carried out on the automated diffractometer DRON 4-07 (NPP "Burevestnik", St. Petersburg) in CuK_α radiation (wavelength is 0,154 nm) under the conditions of Bragg-Brentano focusing θ - 2θ (2θ is the Bragg angle). Current and voltage on the X-ray tube were equal to 20 mA and 40 kV, respectively. For the processing of the experimental results we used the program package DifWin-1 (TOO "Etalon PTTs"). Identification of crystalline phases was realized by the card file JCPDS (Joint Committee on Powder Diffraction Standards).

Calculation of average crystallite sizes was performed by the Selyakov-Scherrer formula as well as by the methods which take into account the influence on the diffraction line physical broadening of small crystallite sizes and deviations of interplanar spacings of the sample from the interplanar spacings of the standard, where microstresses are absent: approximations [19] (approximation of contributions of different factors to physical broadening of diffraction maximums by the Gauss functions or Cauchy functions with their further separation), triple convolution [20] (the best approximating function is used for the description of contribution of each factor).

For calculation of the lattice parameter we used the extrapolation function method. This method allows to extrapolate the value of lattice parameter to the angle $2\theta = 90^\circ$, where error of the determination of interplanar spacings as well as lattice parameter is extremely small. Nelson-Riley [21] function was used as the extrapolation one.

Electron-microscopic and electron-diffraction investigations were carried out after ultrasonic dispersion of the samples on the transmission electron microscope PEM-125K (OAO "SELM", Sumy) at the accelerating voltage of 90 kV and beam current of 100 μA . In the electron-diffraction regime, width of the aperture diaphragm was equal to 0,1 mm, intermediate lenses operated without magnification. Obtained diffraction patterns are presented in Fig. 2, Fig. 3, and Fig. 4.

To remove the polysaccharide component, initial composite samples were annealed in air at 200°C during one hour. Then mineralized composites and samples of "pure" magnetite were placed into distilled water and treated by ultrasound on the plant UZDN-A (OAO "SELM", Sumy). Ultrasonic source was located in vessel with distilled water and powder samples during 10 min. Specific power was about 15-20 W/cm^2 at the source working frequency of 22 kHz. Then several drops of the obtained suspension were coated on the directed upward vertically ultrasonic source UZDN-A and sprayed during 2-3 sec varying the plant power. Sputtered aerosol was caught on thin carbon film (10-20 nm) placed on copper grid for TEM.

Measurements of linear sizes of crystalline magnetite particles and statistical handling of the results were performed using the program VideoTesT-Razmer 5.0 (OOO "VideoTesT", St. Petersburg) [21]. JCPDS data was used for the interpretation of the electron diffraction patterns.

3. RESULTS AND DISCUSSION

According to the X-ray phase analysis data, all studied samples represent magnetite Fe_3O_4 (JCPDS No19-629) with different degree of crystallinity, and crystallite sizes in chitosan/ Fe_3O_4 composites are much less than in Fe_3O_4 synthesized without participation of polysaccharide matrix (Fig. 1).

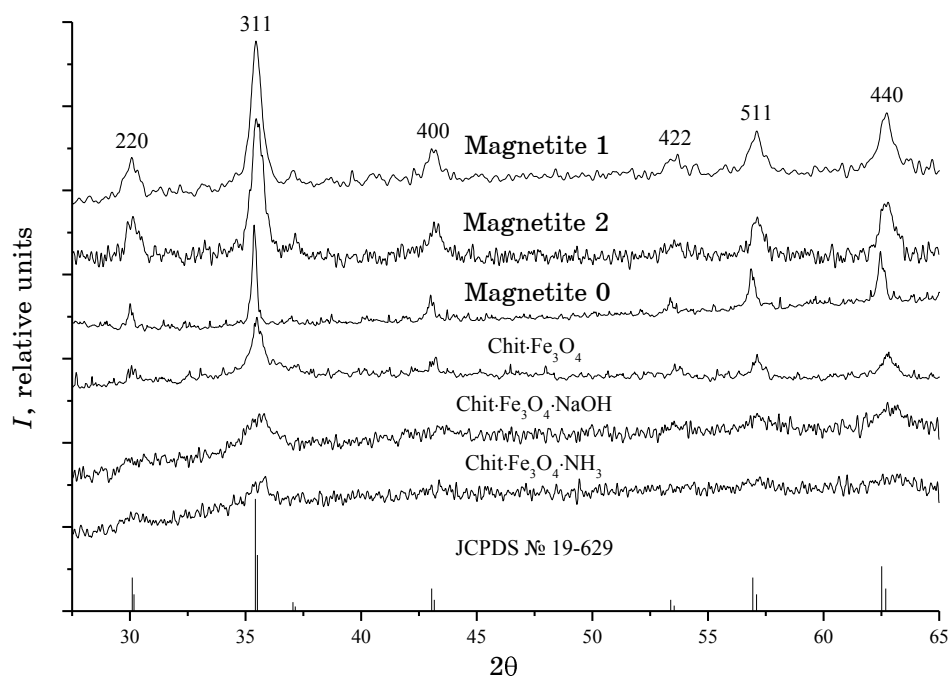


Fig. 1 – X-ray diffraction patterns of magnetite samples. Indexes denote main lines of Fe_3O_4 (JCPDS No19-629), at the bottom – theoretical diffraction pattern of Fe_3O_4

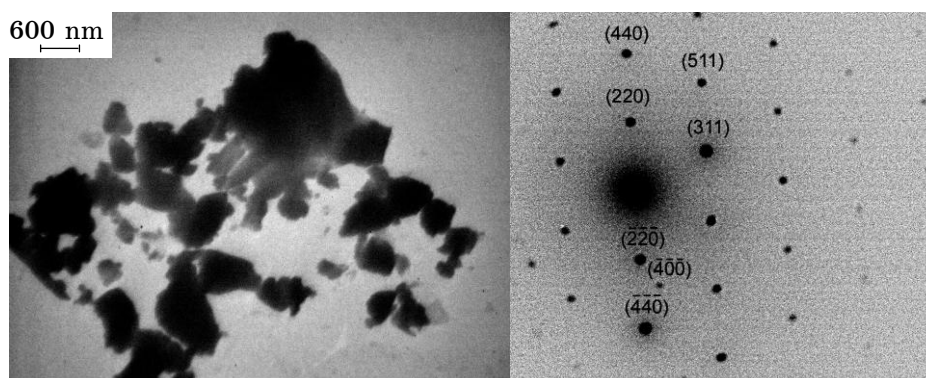
In Table 1 we present the calculation results of the structural and substructural characteristics of magnetite samples using X-ray diffraction data. As seen from this data, there is an interconnection between unit cell parameters and crystallite sizes: decrease in the crystallite sizes during synthesis with the participation of surface agents (polysaccharide matrix) is accompanied by the decrease in the Fe_3O_4 unit cell size. Difference in the values of crystallite sizes calculated by the Selyakov-Scherrer formula for reflexes (220) and (440) can be explained by the significant contribution of lattice microdeformation to the physical broadening of lines, since, as known, high dispersity of crystallites and lattice microdistortions influence differently the angular dependence of the diffraction broadening on a scale of the electron diffraction pattern [19].

Calculation results of the crystallite sizes by the methods of approximation and triple convolution agree satisfactorily, and some quantitative differences are explained by the redistribution of contributions of different factors to the physical broadening of diffraction maximums. In this case, absolute values of lattice microdeformations are rather large (0,005-0,018) and have expressed tendency to the growth at the decrease in the crystallite sizes.

During investigations by the TEM method we have obtained micrographs of aggregates of magnetite nanoparticles at different magnification and micro diffraction patterns. By the TEM and electron diffraction data, sample “Magnetite 0” represented a polydisperse magnetite with the sizes of crystalline particles of 200-600 nm. Electron diffraction patterns from separate crystalline particles of this sample had a view typical for monocrystals (Fig. 2).

Table 1 – Structural and substructural characteristics of magnetite samples by the XRD data

Sample	Lattice parameter by Nelson-Riley, nm	Crystallite sizes by Scherrer	Crystallite sizes and lattice microdeformations			
			approximation method		“triple convolution” method	
		$\langle L \rangle$, nm	$\langle L \rangle$, nm	$\langle \varepsilon \rangle \cdot 10^3$	$\langle L \rangle$, nm	$\langle \varepsilon^2 \rangle^{0.5} \cdot 10^3$
Magnetite 0	0,84013	37,3 (220) 46,7 (440)	31,1	0,8	33,9	0,8
Magnetite 1	0,83767	14,6 (220) 22,2 (440)	10,9	3,5	13,4	2,7
Magnetite 2	0,83688	10,7 (220) 14,2 (440)	8,5	3,4	9,9	3,3
Chit·Fe ₃ O ₄	0,83457	4,1 (220) 7,9 (440)	2,7	17,8	3,8	9,8
Chit·Fe ₃ O ₄ ·NaOH	0,83779	7,0 (220) 5,3 (440)	10,4	6,9	8,3	8,7
Chit·Fe ₃ O ₄ ·NH ₃	0,83553	5,1 (220) 7,4 (440)	3,9	9,1	4,8	7,4

**Fig. 2** – Electron microscopic image of the crystals and micro electron diffraction pattern of magnetite “Magnetite 0”

Electron diffraction patterns of other samples (Fig. 3, Fig. 4) agree well with the XRD data confirming the crystalline nature and phase composition of nanoparticles, and point character of the rings implies that electron beam forms a diffraction pattern on a group (agglomerate) of some small Fe₃O₄ crystals. The corresponding diffraction reflexes of Fe₃O₄ magnetite (JCPDS No19-629) are marked by the Miller indices.

Comparative analysis of the electron microscopy data (for example, Fig. 3, Fig. 4) confirms well the XRD data about the decrease in the sizes of crystalline magnetite particles during synthesis with the participation of surface agents. This is seen on the patterns of electron diffraction: point character of micro electron diffraction patterns is strongly pronounced in the case of relatively large crystals (Fig. 3); and almost solid diffraction rings (Fig. 4) correspond to the smallest crystallite sizes.

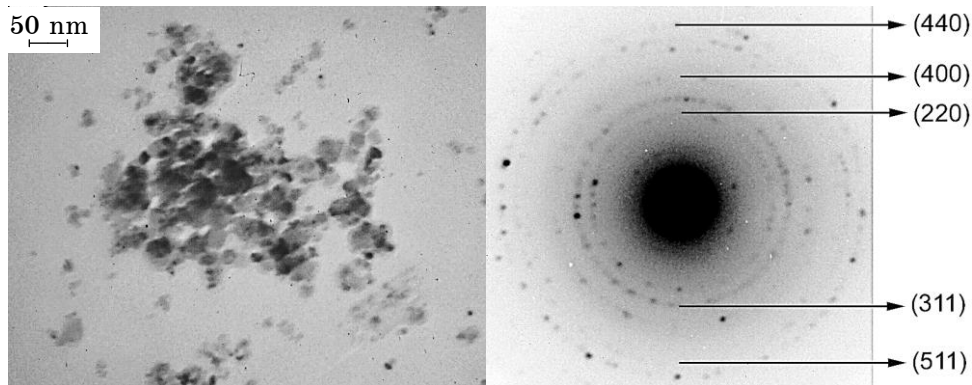


Fig. 3 – Electron microscopic image of the crystals and micro electron diffraction pattern of magnetite “Magnetite 2”

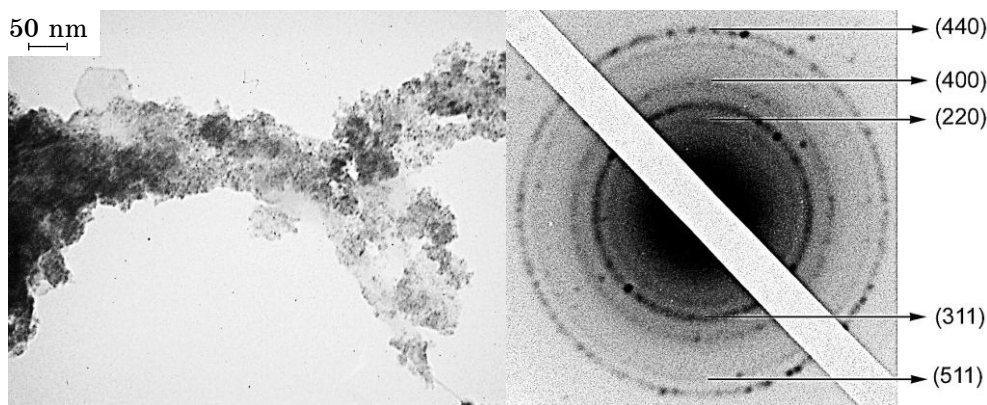


Fig. 4 – Electron microscopic image of the crystals and micro electron diffraction pattern of magnetite “Chit-Fe₃O₄·NaOH”

According to the results of the treatment of microscopic images, we have plotted histograms (Fig. 5) demonstrating the size distribution of crystalline particles. It is seen from the analysis of these histograms that application of codeposition with the participation of polysaccharides and other surface agents leads not only to the decrease in the sizes of magnetite nanoparticles, but also narrows the spread of their values.

For magnetite particles obtained by the codeposition in polysaccharide matrix, the sizes determined from the electron microscopy data (~ 5-10 nm) qualitatively correspond to the average crystallite sizes or coherent-scattering regions obtained from the line broadening of the X-ray diffraction. This allows to assume that such nanoparticles can consist of one magnetic domain, do not have internal boundaries, and, so, rather easy can change the direction of the magnetization.

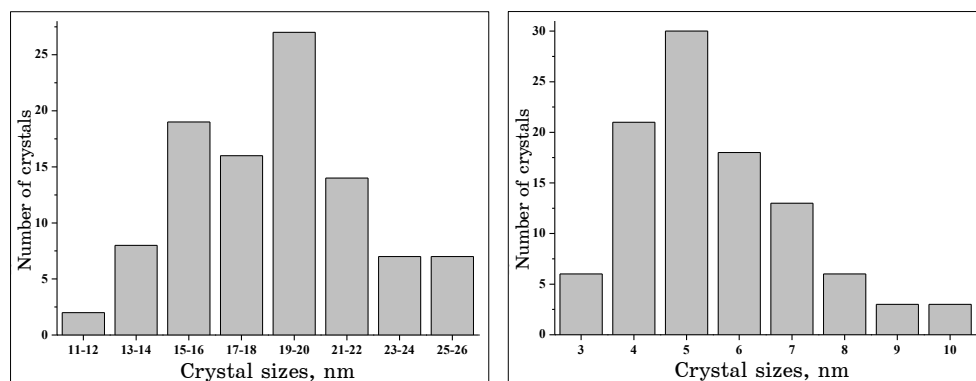


Fig. 5 – Distribution of the particle sizes of magnetite samples in accordance with the TEM data. On the left – “Magnetite 2”, on the right – “Chit-Fe₃O₄·NaOH”

4. CONCLUSIONS

Deposition of magnetite in biopolymer matrix significantly decreases the size of the formed Fe₃O₄ nanoparticles that indicates the chitosan inhibition of the Fe₃O₄ crystal formation and growth processes. Structural and substructural characteristics of Fe₃O₄ nanoparticles synthesized in biopolymer matrix are also sensitive to other changes in the reaction conditions, in particular, to the addition of alkali, ammonia, change in the codeposition temperature.

Results of the determination of the crystallite sizes by the XRD methods satisfactorily agree with direct measurements of nanoparticles by the TEM method for particles with the sizes of 5-20 nm. In the case of large crystalline particles (> 200 nm, sample “Magnetite 0”), sizes measured using TEM are 3-4 times more than crystalline sizes defined by the XRD data. This is explained by the fact that each “large” crystalline particle consists of some crystallites or coherent-scattering regions.

Directed decrease in the Fe₃O₄ nanoparticle sizes by the introduction of biopolymer growth inhibitors, alkali, ammonia, increase in the synthesis temperature is accompanied by the increase in the nanoparticle crystal structure imperfection and decrease in the unit cell sizes. Formation of iron-deficient structure of Fe_{3-δ}O₄ magnetite with violation of the initial Fe³⁺ and Fe²⁺ ion ratio is the most probable process.

Detailed clarification of the structural features of the nanosized magnetite synthesized in biopolymer matrices requires subsequent systematic investigations using complementary tool approaches and involving the determination methods of the magnetic and electrophysical properties which define service characteristics of the given materials.

The authors are grateful to the head of the chair of applied physics of SumDU prof. Protsenko I.E. for the support and fruitful discussions and consultations.

REFERENCES

1. P. Tartaj, M.P. Morales, S. Veintemillas-Verdaguer, et al., *J. Phys. D: Appl. Phys.* **36**, 182 (2003).
2. M.A. Shah, M.S. Al-Shahry, A.M. Asiri, *International Journal of Nano and Biomaterials* **2**, 164 (2009).
3. J. Sun, S. Zhou, P. Hou, et al., *J. Biomed. Mater. Res.* **80A**, 333 (2007).
4. P. Berger, N.B. Adelman, K.J. Beckman, et al., *J. Chem. Educ.* **76**, 943 (1999).
5. G.Q. Zhang, H.P. Wu, M.Y. Ge, et al., *Mater. Lett.* **61**, 2204 (2007).
6. S.M. Ramay, S.A. Siddiqi, M.S. Anwar, et al., *Chinese Phys. Lett.* **26**, 117504 (2009).
7. Y. Wang, B. Li, Y. Zhou, et al., *Nanoscale Res. Lett.* **4**, 1041 (2009).
8. M.A. Garza-Navarro, V.A. Gonzalez-Gonzalez, A. Torres-Castro, et al., *J. Appl. Polym. Sci.* **117**, 785 (2010).
9. J. Giri, S.G. Thakurta, J. Bellare, et al., *J. Magn. Magn. Mater.* **293**, 62 (2005).
10. D.T.K. Dung, T.H. Hai, L.H. Phuc, et al., *J. Phys. Conf. Ser.* **187**, 012036 (2009).
11. P. Sipos, *Rom. Rep. Phys.* **58**, 269 (2006).
12. L. Guo, G. Liu, R.-Y. Hong, et al., *Mar. Drugs* **8**, 2212 (2010).
13. G. Li, Y. Jiang, K. Huang, et al., *J. Alloy Compd.* **466**, 451 (2008).
14. M. Rinaudo, *Prog. Polym. Sci.* **31**, 603 (2006).
15. H. Peniche, C. Peniche, *Polym. Int.* **60**, 883 (2011).
16. A.A. Riccardo, Muzzarelli, *Carbohydr. Polym.* **83**, 1433 (2011).
17. G. Shimmel, *Metodika elektronnoy mikroskopii* (M.: Mir: 1972).
18. Y.D. Yagodkin, S.V. Dobatkin, *Inorg. Mater* **44**, 1520 (2008).
19. A.A. Rusakov, *Rentgenografiya metallov* (M.: Atomizdat: 1977).
20. A.S. Kagan, L.M. Shishlyannikova, A.P. Unikel, *Zavodskaya laboratoriya* **46**, 903 (1980).
21. G. Lipson, G. Stiple, *Interpretatsiya poroshkovyh rentgenogramm* (M.: Mir: 1972).
22. <http://www.videotest.ru>.
23. N.F. Kushchevskaya, *Poroshkovaya metallurgiya* **7**, 1 (1998).